Aberration and self-reconstruction of zero-order Bessel beams in isolated and array format generated using positive and negative axicon lenses

Prasenjit Praharaj, Razvan Stoian, Manoj Kumar Bhuyan

Title Page

1. **Article title:** Aberration and self-reconstruction of zero-order Bessel beams in isolated and array format generated using positive and negative axicon lenses

Abstract: Bessel beam arrays, which can be created involving multiple axicons, diffractive elements, and interference effects, can experience several types of aberrations that distort their ideal characteristics, limiting their applications in microscopy, photonics, and material processing. For instance, Tilt aberration occurs when the individual axicons or optical elements in the Bessel beam array generation setup are misaligned or tilted relative to each other. This tilt can affect the beam's quality, focusing ability, and propagation characteristics. The present study experimentally investigated how any tilt associated with the axicon lens (of both positive and negative surface profile) affects the spatial characteristics of Bessel beams in isolated as well as in array formats. In particular, the aberration characteristics of [1x7] Bessel beam arrays of conical half-angle up to 11 degrees were studied. The spatial filtering of Bessel beam arrays was also demonstrated.
Keywords: Bessel Beam, Optical Array, Aberration, Self-reconstruction, Dammann Grating

2. Full contact details of corresponding author:

Manoj Kumar Bhuyan
CSIR – Central Scientific Instruments Organisation, Sector 30C, Chandigarh 160030, India
&Academy of Scientific and Innovative Research (AcSIR), Ghaziabad 201002, India
Email: manoj.bhuyan@csio.res.in, manoj.femto@gmail.com

3. Complete authors list:

(i) Prasenjit Praharaj
CSIR – Central Scientific Instruments Organisation, Sector 30C, Chandigarh 160030, India
&Academy of Scientific and Innovative Research (AcSIR), Ghaziabad 201002, India
Email:prasenjit.csio21a@acsir.res.in
ORCHID:0000-0001-5269-8875

(ii) Razvan Stoian
Laboratoire Hubert Curien, UMR 5516 CNRS, Université de Lyon, Université Jean Monnet, 42000 Saint Etienne, France
Email: razvan.stoian@univ-st-etienne.fr
ORCHID: 0000-0003-2107-9515

(iii) Manoj Kumar Bhuyan
CSIR – Central Scientific Instruments Organisation, Sector 30C, Chandigarh 160030, India
&Academy of Scientific and Innovative Research (AcSIR), Ghaziabad 201002, India
Email: manoj.bhuyan@csio.res.in, manoj.femto@gmail.com
ORCHID:0000-0001-9757-6994

4. Acknowledgements

This work was supported by the Department of Science and Technology - Science and Engineering Research Board, India [SRG/2020/001538].

5. **Declaration of Interest statement:** The authors declare no conflicts of interest.

Aberration and self-reconstruction of zero-order Bessel beams in isolated and array format generated using positive and negative axicon lenses

Abstract: Bessel beam arrays, which can be created involving multiple axicons, diffractive elements, and interference effects, can experience several types of aberrations that distort their ideal characteristics, limiting their applications in microscopy, photonics, and material processing. For instance, Tilt aberration occurs when the individual axicons or optical elements in the Bessel beam array generation setup are misaligned or tilted relative to each other. This tilt can affect the beam's quality, focusing ability, and propagation characteristics. The present study experimentally investigated how any tilt associated with the axicon lens (of both positive and negative surface profiles) affects the spatial characteristics of Bessel beams in isolated as well as in array formats. In particular, the aberration characteristics of [1x7] Bessel beam arrays of conical half-angle up to 11 degrees were studied. The spatial filtering of Bessel beam arrays was also demonstrated.

Keywords: Bessel Beam, Optical Array, Aberration, Self-reconstruction, Dammann Grating

1. Introduction

The motivation to study aberrations in Bessel beam arrays stems from a wide range of practical concerns, including improving imaging quality, enhancing optical manipulation techniques, advancing communication systems, designing smart manufacturing techniques, and pushing the boundaries of optical engineering. Generally, aberrations of a light beam caused by either off-axis illumination or focusing conditions, significantly degrade the beam's spatial profile, and often reducing the focal depth. Such aberration characteristics thus act as detrimental factors in microscopy and material processing, where precise control over the beam characteristics is mandated [1,2]. Therefore, the aberration effects of primarily the isolated (i.e., single) Gaussian laser beams are widely studied, and indeed many schemes to minimize the effects of aberrations by using adaptive optics, spatial light modulator (SLM) etc. have been proposed [3,4].

The optical beam arrays are eventually emerged as a powerful technology with the potential to enhance beam control (complex beam patterns, multiple beams) and manipulation, often required for LIDAR, free space optical communications [5,6], optical interconnect [7,8], optical trapping [9] and material processing [10–12]. Indeed, the early investigations were primarily focused on the generation of beam arrays of Gaussian spatial features using diffractive optical elements (DOE), SLM, lenslet array and grating. In order to further enhance the potential of beam array technology, recently interests have been aroused towards realizing array of non-diffractive beams such as Bessel beams, Airy beams etc. [13–17] with self-reconstruction ability [18]. For instance, S. Orlov et al. [19] have demonstrated array of Bessel-like beams with independent axial intensity distributions. The array concept was also exploited for the realization of parallel vortical optical needle beams [20,21]. Nevertheless, to understand the limitations of beam array technology, it is imperative to study the aberration characteristics of optical beams in array configurations.

Among the different classes of non-diffracting beams, Bessel beams stand out in terms of their remarkable spatial characteristics [13]. For instance, zero-order Bessel beams have a narrow central spot that maintains reasonable intensity over a long propagation distance and have exceptional stability in nonlinear propagation

Abbreviations: CW = Continuous Wave, SLM= Spatial Light Modulator, FWHM= Full Width at Half Maximum

regimes. These properties make them ideal, especially for applications like material processing, optical trapping, microscopy, and plasma physics [13,22–28]. Such beams can be generated using annular aperture, axicon lens, SLM, DOE etc. Because of its passive in nature, ease of use and high throughput, axicon lens is found in most Bessel beam generation arrangements [29]. Researchers have explored axicon lenses with various surface profiles [30–33]. For instance, axicon lenses with negative surface profiles were used to generate high cone angle Bessel beams, potentially useful in material processing and plasma physics [30–32]. It is worth noting that similar to a spherical lens, any off-axis illumination of axicon lens can introduce aberration into the generated Bessel beams; the corresponding radial symmetry gets distorted and effective depth of focus also gets reduced [34]. This becomes a concern, especially in scanning systems that rely on axicon lenses, as even slight deviations from perfect alignment can lead to aberrated Bessel beams, degrading the system performance [25].

The impact of aberrations on isolated Bessel beams was therefore studied by several researchers [35–39]. For example, Thaning et al. showed that tilting a circular axicon lens during illumination, which would generate aberrated Bessel beams, has the same effect as using an elliptical axicon lens with straight-on illumination [39]. Jaroszewicz et al. capitalized on this concept, demonstrating aberration correction using an axicon with a fixed level of ellipticity controlled by SLM [36]. Cheng et al. further developed this idea, achieving aberration correction with variable ellipticity via an SLM [38]. This approach to aberration compensation has even been applied in glass processing [40,41].

Although several efforts were made to understand the aberration characteristics of Bessel beams, it was primarily with single Bessel beams. However, the aberration effects were never studied for Bessel beam arrays [42–45], which can be a potential tool for applications in the fields of parallel material processing, microscopy, and plasma physics. Therefore, the present study aims to investigate the aberration characteristics of Bessel beam arrays generated using axicon lenses of different surface profiles i.e., positive and negative, in combination with a telescopic arrangement. For sake of comparison, the aberration characteristics of single Bessel beams were also studied.

2. Experimental setups and results

The experimental setups were developed to generate zero-order Bessel beams in isolated and array format and to evaluate their spatial characteristics. For instance, Fig. 1(a) shows a typical setup used for the generation of high cone angle Bessel beams using a “positive” axicon lens. The Gaussian CW laser beams of 532 nm wavelength were first incident on a polymer linear-phase, positive axicon lens of 177-degree apex angle. Such an arrangement generates low cone angle Bessel beams. The generated Bessel beams were further de-magnified (Magnification, M = 1/16.6) using a telescope consisting of a plano-convex lens-1 (f=150 mm) and an objective lens -2 (20X/0.4 NA). Such an arrangement thus generates high cone angle Bessel beams in the focal region of objective lens-2. In order to reveal the spatial characteristics of the generated high cone angle Bessel beams, a magnification system (M=32) comprising of a plano-convex lens-3 (f=150 mm) and an objective lens-4 (20X/0.4 NA) coupled with a CMOS camera (Pixel size = 3.45 µm) was employed. A series of radial (R) cross-sectional profiles of Bessel beams were recorded (camera exposure time of 0.5 ms) along the beam propagation direction (Z-axis) with a longitudinal resolution (dZ) of 5 µm. The recorded radial beam profiles were further processed using MATLAB software to obtain the spatial characteristics of resultant Bessel beams. These beam

Abbreviations: CW = Continuous Wave, SLM= Spatial Light Modulator, FWHM= Full Width at Half Maximum

generation and characterization methods were the same for both single and arrayed Bessel beams. Both positive and negative surface profiles of axicon lenses were considered for beam generation. In addition to this, a grating was placed before the axicon lens in the case of Bessel beam array generation. In the following, the Bessel beam characteristics under various experimental conditions are discussed.

2.1 Positive axicon lens-based Bessel beam generation:

As described above, a "positive" axicon lens (177° apex angle) was employed in combination with a suitable telescope to generate micro-Bessel beams. Fig. 1 (b) shows a longitudinal (R-Z) profile of generated Bessel beams of conical half-angle of 11° with a central core size (full width at half-maxima-FWHM) of 1 µm and non-diffractive FWHM distance of 315 µm. The aberration characteristics of such Bessel beams were further studied. To do so, keeping all other optical elements and their positions the same, the axicon lens (mounted on a rotational stage of 2-degree resolution) was rotated/tilted with respect to its normal illumination position. In the present case, the axicon tilt angles varied in the range of zero to 16 degrees, and corresponding Bessel beam profiles were recorded. Fig. 1(b-e) shows the R-Z profiles of Bessel beams corresponding to α = 0, 8, 12, and 16 degrees respectively. The corresponding radial profiles at a fixed longitudinal position, i.e., Z1 = 255 µm, are shown in Fig. 1(f-i). It is evident from the figure that the radial profile gets distorted from a concentric-ring pattern to a diamond-shaped pattern upon increasing the tilt of the axicon lens, as reported earlier by several researchers [35–39]. This beam profile transformation starts from the tail of Bessel beams. For instance, if the laser beam propagates from the left to right direction, then the beam distortion starts from right to left when the axicon is tilted. The beam profiles shown in Fig. 1(h,i) clearly advocate the above phenomena. Additionally, a lateral shift in the position of the entire Bessel beam was observed when the beam was generated using a tilted axicon lens. A quantitative analysis showed no significant change in the Bessel beam radial profile over the entire non-diffractive zone occurs for $\alpha < 8°$. In contrast, for $\alpha > 8°$, the radial beam profiles start to distort along the non-diffractive zone, starting from the tail; central core intensity drops, and outer ring intensity enhances, as evident from the insets to Fig. 1(h,i). In other words, it can be said that the longitudinal non-diffractive distance reduces with increasing axicon tilt angle.

2.2 Negative axicon lens-based Bessel beam generation:

The Bessel beam can be generated not only using a positive axicon lens but also using a negative axicon lens. The only difference between both cases is the beam evolution pattern. For instance, Ray 1, i.e., marginal rays of input Gaussian beam meet at the "end-point" of Bessel beams that are generated using a positive axicon lens followed by a telescope, as evident from Fig. 1(a). In such case, Ray 2, i.e., central light rays, meet at the "start-point" of Bessel beams. In contrast, Ray 1 meets at the "start-point" of Bessel beams that are generated using a negative axicon lens followed by a telescope, as evident from Fig. 2(a). In such case, Ray 2 meets at the "end-point" of Bessel beams. Basically, the start- and end-points of Bessel beams flip with respect to the surface profiles of the axicon lens. In the present study, Bessel beams were also generated using a negative axicon lens (177.8° apex angle) in combination with a suitable telescope. Fig. 2(b) shows a longitudinal profile of generated Bessel beams of conical half-angle of 9.5° with a FWHM central core size of 1.2 µm and non-diffractive FWHM distance of 340 µm. The aberration characteristics of such Bessel beams were further studied. To do so, keeping all other optical elements and their positions the same, the negative axicon lens was tilted (up to 16°) with respect to its normal illumination position, and corresponding Bessel beam profiles were recorded. Fig.

Abbreviations: CW = Continuous Wave, SLM= Spatial Light Modulator, FWHM= Full Width at Half Maximum

2(b-e) shows the R-Z profiles of Bessel beams corresponding to α = 0, 8, 12, and 16 degrees respectively. The corresponding radial profiles at a fixed longitudinal position, i.e., Z1 = - 175 µm, are shown in Fig. 2(f-i).

Like the positive axicon lens, the "distorted radial profile" and "lateral beam shifting" were also observed in the case of tilted negative axicon lens-generated Bessel beams. In this case, also, the beam profile distortion, i.e., from a concentric- ring to a diamond-shaped pattern, starts from the end-point of Bessel beams. Interestingly, the laser beam propagates from left to right direction, and the beam distortion also begins from left to right. The radial beam profiles (captured at Z2 = - 300 µm) shown in Fig. 2(h,i) clearly advocate the above phenomena. From a quantitative analysis, it was also observed that no significant change in the Bessel beam radial profiles over the entire non-diffractive zone occurs for α< 8°. In contrast, for α> 8°, the radial beam profiles start to distort along the non-diffractive zone, starting from the tail-point; the central core intensity drops and the outer ring intensity enhances, as evident from the insets to Fig. 2 (h,i). The longitudinal non-diffractive distance also reduces with increasing axicon tilt angle.

2.3 Positive axicon lens- and grating-based Bessel beam array generation:

An array of Bessel beams can be generated using passive optical elements such as Dammann-like grating and axicon lens [23,42,43]. Here, we followed the array generation method described in Ref. [42]. At first, one-dimensional Dammann-like gratings on the front surface of 3 mm thick soda lime glass materials were machined using a nanosecond pulsed laser. The grating period was maintained at 200 µm with a transition point of 0.5. Fig. 3(a) shows a typical setup used for the generation of an array of high cone angle Bessel beams using the grating as mentioned above, a positive axicon lens (177° apex angle), and a telescope (same as shown in Fig. 1(a)). A Gaussian CW laser beam of 532 nm wavelength was incident on the grating, followed by all other considered optical elements. A high cone angle Bessel beam array was thus generated in the focal zone of objective lens-2. The beam imaging setup and procedure were the same for the entire study. Fig. 3(b) shows a longitudinal (R-Z) profile of the generated array ([1x7] dimension) of Bessel beams of conical half-angle of 11 degrees with FWHM central core size of 1 µm and non-diffractive FWHM distance of 315 µm. The intensities of different diffracted orders of light (Bessel beams) are not uniform, although the uniformity can be maintained by using phase grating [46] instead of amplitude grating as in the present case. In particular, the intensity of third-order diffracted light is relatively low compared to other diffracted orders. The diverging angle, i.e., between zero- and third-order light, was observed to be 6.6 degrees. It was also observed that the Bessel beam spatial characteristics are approximately the same whether it is in isolated (i.e., single) or in array format.

Further, the aberration characteristics of the generated Bessel beam array were studied. In this case, keeping all other optical elements and their positions the same, the positive axicon lens was tilted (up to 16°) with respect to its normal illumination position, and corresponding Bessel beam radial profiles were recorded. Fig. 3(b-e) shows the R-Z profiles of Bessel beam arrays corresponding to the axicon tilts of 0°, 8°, 12° and 16° respectively. The corresponding radial profiles at a fixed longitudinal position, i.e., Z = 265 µm, are shown in Fig. 3(f-i). As with aberrated (i.e., when the axicon lens is tilted), isolated-Bessel beams, the aberrated, arrayed-Bessel beams have distorted radial patterns in each diffracted order of light (i.e., beamlets). In each beamlet, the beam profile transformation (from concentric ring to diamond pattern) starts from the tail of Bessel beams, i.e., the opposite direction of beam propagation. It is also evident from Fig. 3 that the lateral shift in the entire Bessel beam array does occur in the case of a tilted axicon lens. The longitudinal non-diffractive distance of individual

Abbreviations: CW = Continuous Wave, SLM= Spatial Light Modulator, FWHM= Full Width at Half Maximum

Bessel beams of the array also reduces with increasing axicon tilt angle, similar to the case of aberrated, isolated Bessel beams.

2.4 Negative axicon lens- and grating-based Bessel beam array generation:

An array of high cone angle Bessel beams was also generated using a grating (200 μm period and transition point of 0.5), a negative axicon lens (177.8˚ apex angle), and a telescope (same for the entire study) as illustrated in Fig. 4 (a). The beam imaging setup and procedure were the same for the entire study. A Gaussian CW laser beam of 532 nm wavelength was used for beam characteristics evaluation. Fig. 4(b) shows a longitudinal profile of a "negative" axicon lens-generated array ([1x5] dimension) of Bessel beams of conical half-angle of 9.5° with a FWHM central core size of 1.2 μm and non-diffracting FWHM distance of 340 μm. It was also observed that the Bessel beam spatial characteristics are approximately the same whether in isolated or array format. The aberration characteristics of such Bessel beam arrays were further studied. In this case, keeping all other optical element positions the same, the "negative" axicon lens was tilted (up to 16°) with respect to its normal illumination position, and corresponding Bessel beam radial profiles were recorded.

Fig. 4(b-e) shows the R-Z profiles of Bessel beam arrays corresponding to the axicon tilts of 0, 8, 12, and 16 degrees, respectively. The corresponding radial profiles at a fixed longitudinal position, i.e., Z = -310 μm, are shown in Fig. 4(f-i). As with aberrated (i.e., when the axicon lens is tilted), isolated-Bessel beams, the aberrated, arrayed-Bessel beams have distorted radial patterns in each beamlet where the beam profile transformation (from concentric-ring to diamond-pattern) starts from the tail of Bessel beams, i.e., along the beam propagation direction. It is also evident from Fig. 4 that the lateral shift in the entire Bessel beam array does occur in the case of a tilted axicon lens. The longitudinal non-diffractive distance of individual Bessel beams of the array also reduces with increasing axicon tilt angle.

2.5 Self-reconstruction property of Bessel beams:

Self-reconstruction is an important property of non-diffractive optical beams [18]. Here, we studied this property of zero-order Bessel beams. The isolated (i.e., single) and arrayed Bessel beams were generated using suitable optics, as discussed in earlier sections (see Fig. 1(a) and Fig. 3(a)). In this case, an additional obstacle (200 μm wide, square-shaped) was placed next to the axicon lens, keeping all other optical elements the same as illustrated in Fig. 5(a). The beam imaging modality was the same for the entire study. Fig. 5(b) and (c) show the longitudinal (R-Z) profiles of the generated Bessel beams of conical half-angle of 11 degrees corresponding to both unobstructed and obstructed conditions, respectively. It is clearly evident from the figures that the Bessel beams self-reconstruct after 100 μm (obstruction zone) after encountering an obstacle. Fig. 5(d) illustrates such phenomenon of self-reconstruction. The same phenomenon was also observed in the case of the Bessel beam array. Fig. 5(e) shows a longitudinal (R-Z) profile of the generated diverging array ([1x7] dimension) of Bessel beams of conical half-angle of 11 degrees. When such an array encounters with an obstacle placed at the center of the beam, i.e., along the 0-th order diffraction, the obstruction zone (OZ) appears as evident from Fig. 5(f). Indeed, the central Bessel beams self-reconstruct after 100 μm. Note here that no change in the Bessel beam profiles of other beamlets of the array was observed. Similarly, when the obstacle was placed off-axis, the obstruction zone appeared only along the 1-st order diffraction of the beam array, as evident from Fig. 5(g).

Abbreviations: CW = Continuous Wave, SLM= Spatial Light Modulator, FWHM= Full Width at Half Maximum

3. Discussions

As demonstrated in the present study, the zero-order Bessel beams can be generated using refractive-type axicon lenses of both positive and negative surface profiles. One striking feature that was observed in the case of the negative axicon lens was the beam evolution pattern opposite to that of the positive axicon lens. One may note here that there is an advantage in using a negative axicon lens for Bessel beam generation. In this case, no Bessel beams form right after the negative axicon lens, unlike in the case of a positive axicon, where Bessel beams form right from the tip of the axicon lens. Such a situation is expected to be advantageous when ultrashort laser pulses are used, especially for laser material processing. This is because the intense Bessel central core may ablate the convex lens that follows the axicon lens. It's worth noting here that obtaining a negative axicon with sharp depression at its center is a challenging mechanical fabrication job [30]. Interestingly, non-perfect i.e., oblate-tip, positive axicon lenses, have also found applications in material processing due to asymmetry in the beam profile [47]. Such appealing applications thus motivate researchers to design strategies for more generalized asymmetric Bessel beam generation [48,49]. The array of Bessel beams can be generated by several means, as reported in the literature [42–45]. In the present study, arrays ([1x7] dimension) of Bessel beams were produced using both types of axicon lenses in combination with Dammann-like grating and telescope. Such an arrangement provides the flexibility to obtain a Bessel beam array at any desired position, which would otherwise start next to the optical elements, such as metasurface-based axicon [44].

The aberration phenomenon is generally known for its detrimental effect on beam quality. Here, four primary observations related to zero-order Bessel beams of high-cone angles up to 11 degrees were made. (i) The radial profile of Bessel beams gets distorted (i.e., from concentric ring to diamond-shaped profile) when the laser beam propagates through a tilted axicon lens irrespective of its surface profile, i.e., positive or negative. (ii) The non-diffractive length of Bessel beams gets reduced with increasing tilt angle of both positive and negative axicon lenses, as evident from Fig. 6. Here, the non-diffractive length is normalized (i.e., with respect to the non-aberrated Bessel beams), for better comparison between positive and negative axicon lenses. There was also a surprising observation on the aberration of Bessel beams generated using a negative axicon lens. In this case, the non-diffractive length diminishes faster than positive axicon lens-generated Bessel beams. This may be partially due to any manufacturing defect associated with negative axicon lens fabrication. (iii) The spatial characteristics, such as the central core size of generated Bessel beams, remain conserved in either case, i.e., isolated and array format. The flipped beam evolution pattern in the case of the negative axicon lens was also seen in the relevant Bessel beam array. (iv) The aberrated beams, i.e., both isolated and arrayed Bessel beams, were observed to be displaced laterally with respect to the non-aberrated (i.e., zero axicon tilt) beams. For example, a lateral shift of about 32 μm was observed in the case of aberrated Bessel beams due to the positive axicon tilt of 16 degrees. The magnitude of the lateral shift was observed to be the same in both isolated and array Bessel beams.

The self-reconstruction phenomenon (i.e., regeneration of beams after encountering an obstacle) of zero-order Bessel beams is beneficial in laser processing and microscopy applications, where many undesired sample contaminants exist. Such contaminants may obstruct the incident Bessel beams. Indeed, we observed such a phenomenon where the Bessel beams got obstructed by an obstacle but fully regenerated after 100 μm of propagation. This robustness to obstacle encounters can also be observed in the case of the Bessel beam array.

Abbreviations: CW = Continuous Wave, SLM= Spatial Light Modulator, FWHM= Full Width at Half Maximum

We experimentally observed the beam reconstruction in various beamlets of the array, i.e., along different diffraction orders. This observation testifies the fact that obstacle encounters in one beam do not alter the beam characteristics of other beams in an array, as would be needed for parallel processing applications. As the beam obstruction occurs over a certain propagation distance, which depends on the lateral size of obstacle, one may exploit this feature for spatial filtering of beamlets in the array format. For instance, three square-shaped obstacles (i.e., glass plate with laser machined opaque area) of 50, 200 and 500 μm wide were placed at longitudinal positions of 10 mm, 50 mm and 150 mm respectively with respect to the axicon lens; this arrangement resulted into an array of Bessel beams almost without the central Bessel beam as evident from Fig. 7 (a, c). This spatial filtering method was further exploited for complete suppression of negative diffraction orders by suitably placing an obstacle (i.e., 75 mm long slab) in an off-axis manner. Fig. 7(b, d) show the longitudinal profile image of Bessel beam array with only positive orders of diffraction. Such spatial filtering arrangement thus may enable new light-matter interaction geometries involving multiple Bessel beams of desired configuration, with potential applications in optical tweezers, material processing and nonlinear optics.

4. Conclusion

Zero-order Bessel beams in isolated and array format were experimentally generated primarily using refractive type axicon lens of both “positive” and “negative” surface profiles. In particular, Bessel beams of conical half-angle up to 11 degrees and an array of [1×7] dimensions were obtained using a 200 μm period, one-dimensional Dammann-like grating combined with an axicon lens of 177-degree apex angle. Towards understanding the robustness of generated high cone angle Bessel beams, the aberration effect was studied. It was observed that the Bessel beams, whether they are in isolated or in array format, retain the typical concentric-ring type radial profile until 8 degrees of axicon tilt angles, setting a tolerance limit. We, therefore, anticipate that the aberration results would significantly help in designing future machining and microscopy experiments. The robustness of Bessel beams against obstacle encounters was also evident from the self-reconstruction studies, where any Bessel beam in an array could recover the typical Bessel radial pattern after a certain regeneration length. We further demonstrated that using spatial filtering i.e., with the help of suitable beam blocks after the axicon lens, one may selectively isolate different beamlets of an array.

Abbreviations: CW = Continuous Wave, SLM= Spatial Light Modulator, FWHM= Full Width at Half Maximum

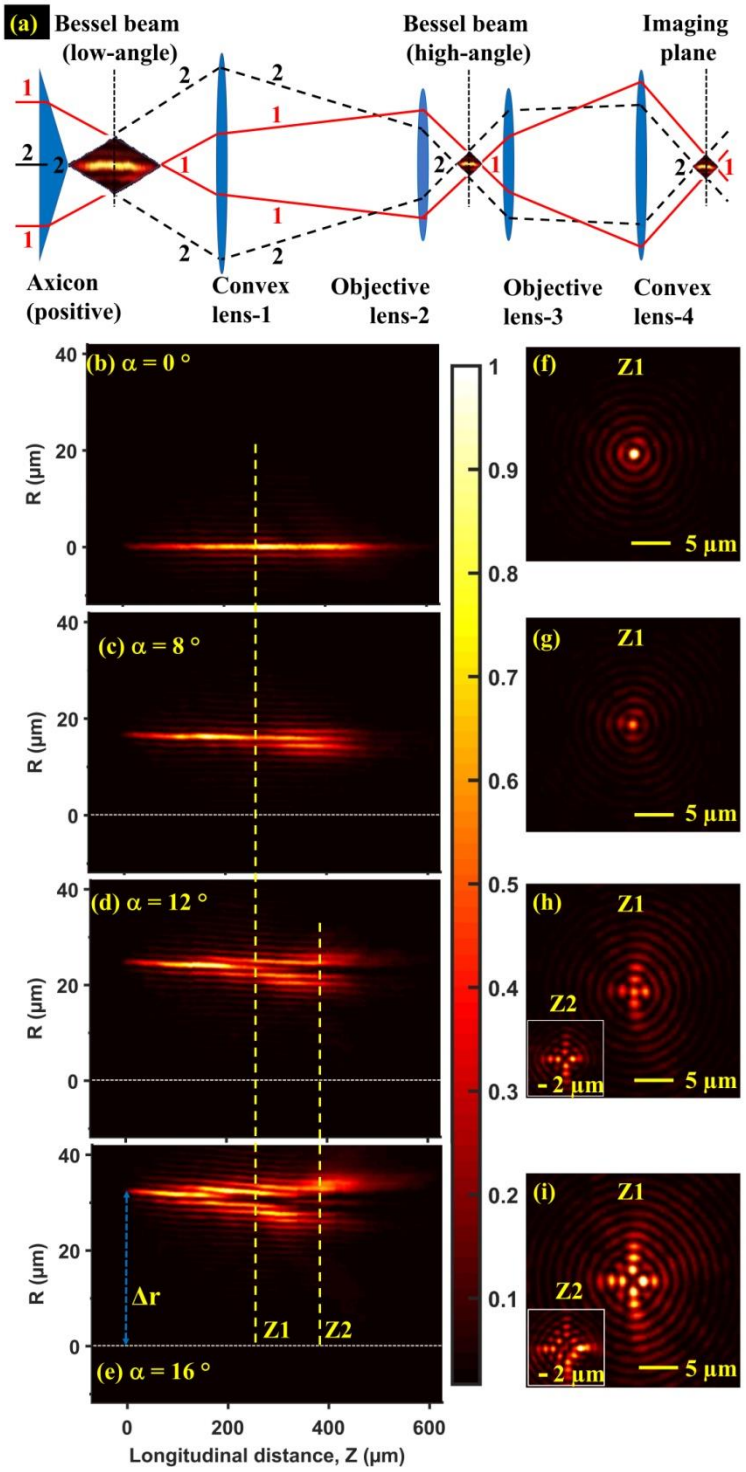

Fig. 1.(a) Illustrative diagram of zero-order Bessel beam generation using positive axicon lens. Ray 1 and Ray 2 correspond to the light rays that propagate along the marginal and central axis, respectively. The longitudinal (R-Z) cross-sectional profile images of generated Bessel beams of 11° conical half-angle corresponding to various axicon tilt angles are shown as follows: (b) α = 0°, (c) α = 8°, (d) α = 12°, and (e) α = 16°. (f-i) The radial cross-sectional profiles of Bessel beams at fixed longitudinal distances, i.e., Z1= 255 μm and Z2= 380 μm (insets), are shown for all considered axicon tilt positions.

Abbreviations: CW = Continuous Wave, SLM= Spatial Light Modulator, FWHM= Full Width at Half Maximum

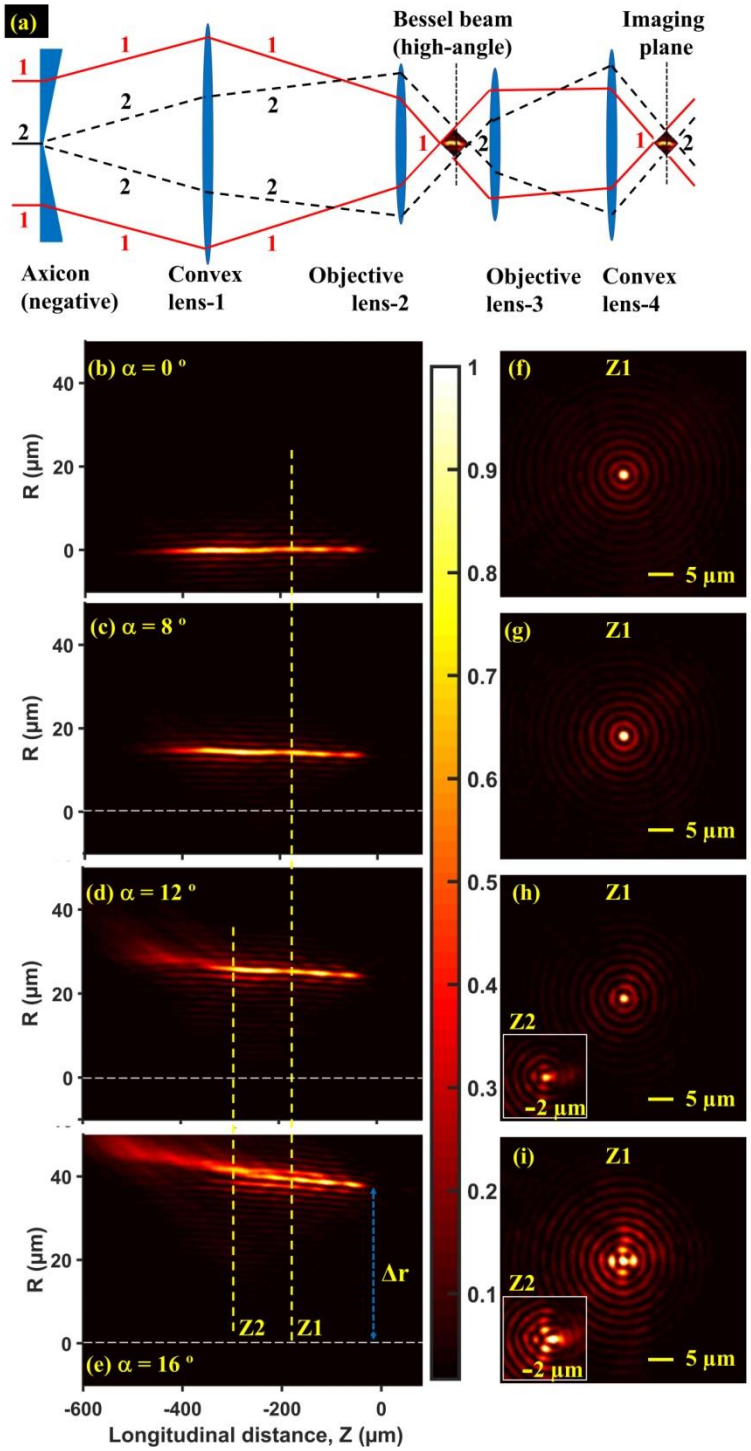

Fig. 2. (a). Illustrative diagram of zero-order Bessel beam generation using negative axicon lens. Ray 1 and Ray 2 correspond to the light rays that propagate along the marginal and central axis, respectively. The longitudinal (R-Z) cross-sectional profile images of generated Bessel beams of 9.5° conical half-angle corresponding to various axicon tilt angles are shown as follows: (b) α = 0°, (c) α = 8°, (d) α = 12°, and (e) α = 16°. (f-i) The radial cross-sectional profiles of Bessel beams at fixed longitudinal distances, i.e., Z1= - 175 μm and Z2= - 300 μm (insets), are shown for all considered axicon tilt positions.

Abbreviations: CW = Continuous Wave, SLM= Spatial Light Modulator, FWHM= Full Width at Half Maximum

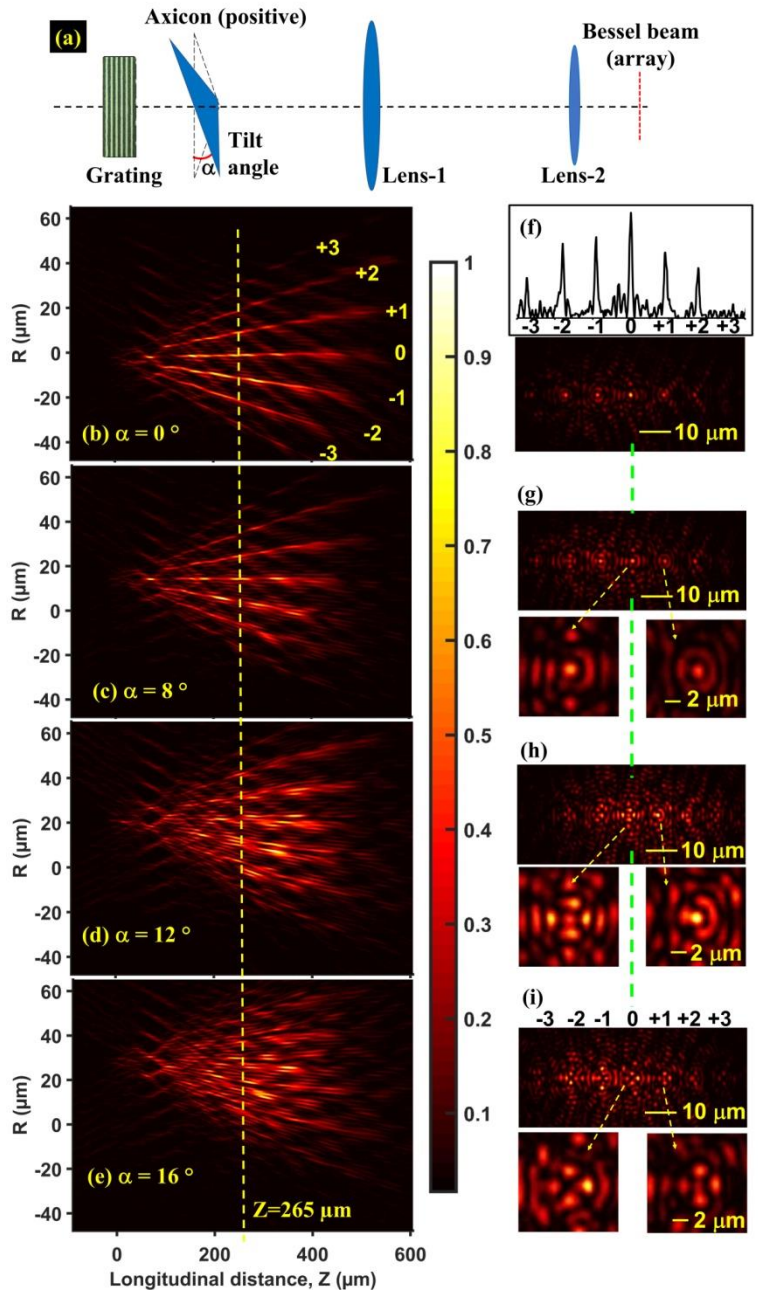

Fig. 3. (a) Illustrative diagram of zero-order Bessel beam array generation using Dammann-like grating of 200 μm period, positive axicon lens, and a telescope. The longitudinal (R-Z) cross-sectional profile images of a generated array of Bessel beams of 11° conical half-angle corresponding to various axicon tilt angles (α) are shown as follows: (b) α = 0°, (c) α = 8°, (d) α = 12°, and (e) α = 16°. (f-i) The radial cross-sectional profiles of Bessel beams at a fixed longitudinal distance, i.e., Z = 265 μm, are shown for all considered axicon tilt positions. The zoomed images of zero-order and first-order diffracted beams are also shown as insets.

Abbreviations: CW = Continuous Wave, SLM= Spatial Light Modulator, FWHM= Full Width at Half Maximum

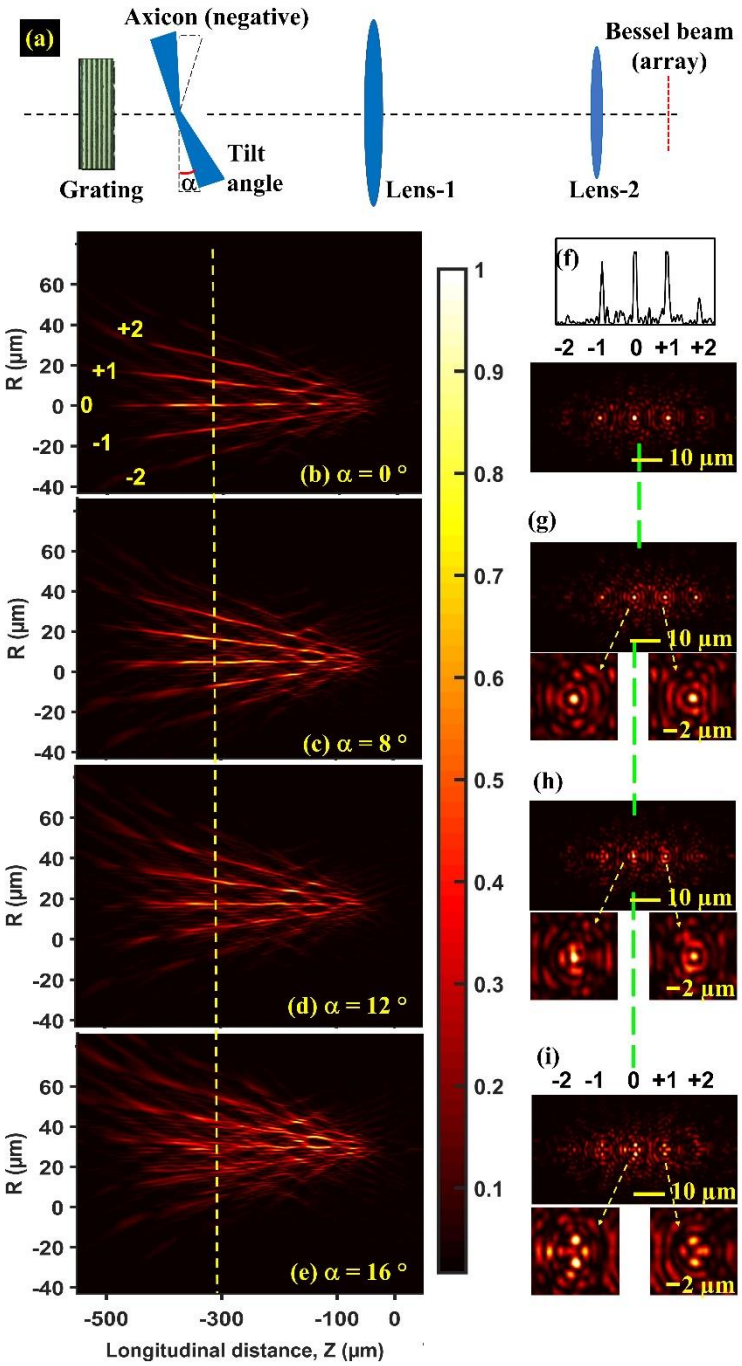

Fig. 4. An illustrative diagram of zero-order Bessel beam array generation using Dammann-like grating of 200 μm period, negative axicon lens, and a telescope is shown in (a). The longitudinal cross-sectional profile images of the generated array of Bessel beams of 9.5° conical half-angle corresponding to various axicon tilt angles (α) are shown as follows: (b) α = 0°, (c) α = 8°, (d) α = 12°, and (e) α = 16°. (f-i) The radial cross-sectional profiles of Bessel beams at a fixed Z = - 310 μm are shown for all considered axicon tilt positions.

Abbreviations: CW = Continuous Wave, SLM= Spatial Light Modulator, FWHM= Full Width at Half Maximum

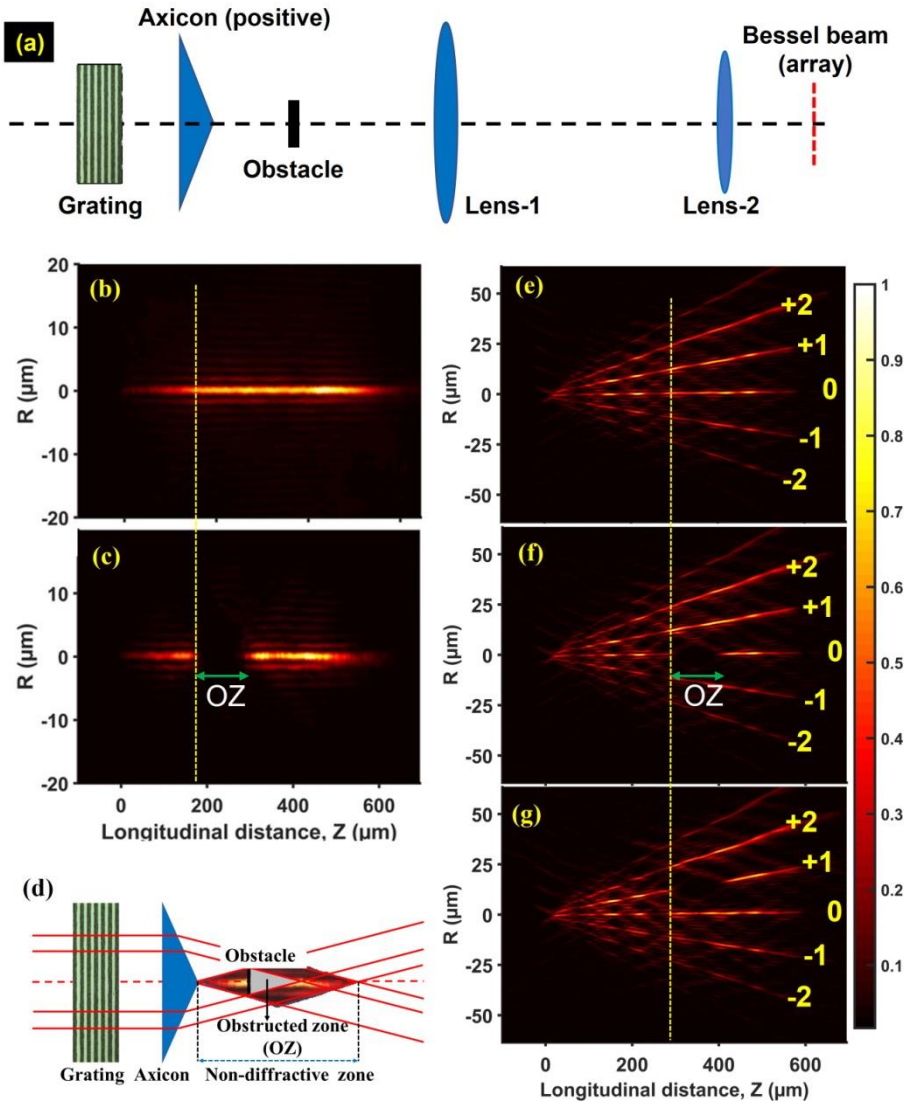

Fig. 5. Self-reconstruction property of zero-order Bessel beams. An illustrative diagram of the Bessel beam (11° conical half-angle) generation setup is shown in (a). The longitudinal cross-sectional profile images of the generated, isolated (single) Bessel beams corresponding to both unobstructed and obstructed conditions are shown in (b) and (c), respectively. (d) An illustrative diagram of obstacle presence within the axicon lens-generated Bessel beams. The longitudinal cross-sectional profile images of the array [1x7] of Bessel beams corresponding to various unobstructed and obstructed conditions are shown in (e-g). (f) and (g) represent the cases where the obstacle was present along the 0-th order and 1-st order diffraction, respectively.

Abbreviations: CW = Continuous Wave, SLM= Spatial Light Modulator, FWHM= Full Width at Half Maximum

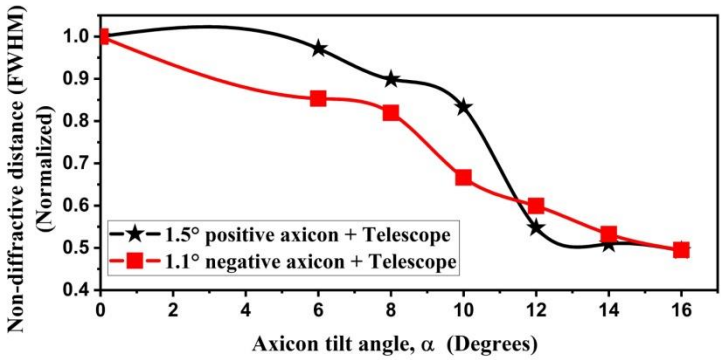

Fig. 6. Longitudinal non-diffractive distance (normalized) variation of aberrated Bessel beams generated using positive and negative axicon lenses. The normalization was done with respect to the non-aberrated (i.e., zero axicon tilt angle) Bessel beams.

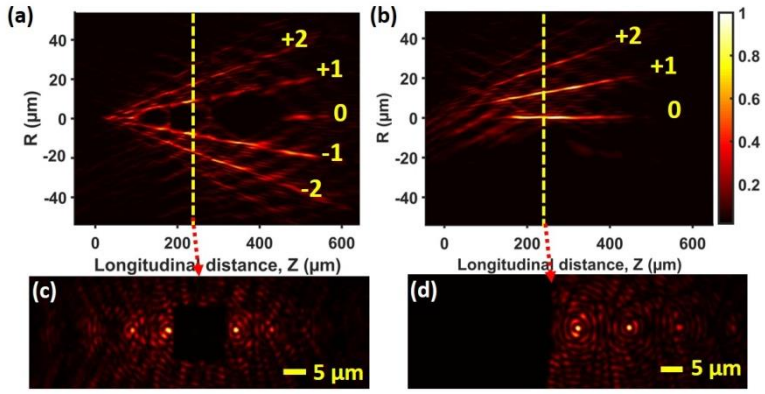

Fig. 7. Demonstration of selection of diffraction orders via spatial filtering in case of Bessel beam array (11° Bessel conical half-angle, [1x7] array format). (a) The longitudinal cross-sectional profile image of the generated Bessel beam array with significant suppression of central beam. (b) The longitudinal cross-sectional profile image of the generated Bessel beam array with suppression of negative diffraction orders. The respective radial cross-sectional profiles of Bessel beam arrays recorded at Z = 240 μm are shown in (c) and (d).

Data availability.

Data will be made available on request.

References

[1] N. Li, F. Luo, C. Yang, Z. Peng, L. Xuan, Q. Bu, Q. Mu, X. Zhang, The Effects of Optical Aberrations to Illumination Beam Thickness in Two-Photon Excitation Microscopes, Applied Sciences 12 (2022) 7156. https://doi.org/10.3390/APP12147156.

[2] K. Cvecek, I. Miyamoto, M. Adam, M. Schmidt, Effects of Spherical Aberrations on Micro Welding of Glass using Ultra Short Laser Pulses, Phys Procedia 39 (2012) 563–568. https://doi.org/10.1016/J.PHPRO.2012.10.074.

[3] M. Schwertner, M.J. Booth, T. Tanaka, T. Wilson, S. Kawata, Spherical aberration correction system using an adaptive optics deformable mirror, Opt Commun 263 (2006) 147–151. https://doi.org/10.1016/J.OPTCOM.2006.01.026.

[4] J. Arines, V. Durán, Z. Jaroszewicz, J. Ares, E. Tajahuerce, P. Prado, J. Lancis, S. Bará, V. Climent, Measurement and compensation of optical aberrations using a single spatial light modulator, Opt Express 15 (2007) 15287–15292. https://doi.org/10.1364/OE.15.015287.

[5] R.L. Morrison, S.L. Walker, T.J. Cloonan, Beam array generation and holographic interconnections in a free-space optical switching network, Appl Opt 32 (1993) 2512–2518. https://doi.org/10.1364/AO.32.002512.

[6] Y. Wu, S. Shao, Y. Li, X. Chen, D. Che, J. Chen, K. Du, R. Jiang, X. Huang, D. Kan, Multi-beam optical phase array for long-range LiDAR and free-space data communication, Opt Laser Technol 151 (2022) 108027. https://doi.org/10.1016/J.OPTLASTEC.2022.108027.

Abbreviations: CW = Continuous Wave, SLM= Spatial Light Modulator, FWHM= Full Width at Half Maximum

[7] S.H. Song, J.S. Jeong, E.H. Lee, Beam-array combination with planar integrated optics for three-dimensional multistage interconnection networks, Appl Opt 36 (1997) 5728–5731. https://doi.org/10.1364/AO.36.005728.
[8] C. Yu, M.R. Wang, A.J. Varela, B. Chen, High-density non-diffracting beam array for optical interconnection, Opt Commun 177 (2000) 369–376. https://doi.org/10.1016/S0030-4018(00)00583-6.
[9] R.L. Eriksen, V.R. Daria, J. Glückstad, Fully dynamic multiple-beam optical tweezers, Opt Express 10 (2002) 597–602. https://doi.org/10.1364/OE.10.000597.
[10] G. Liang, S. Sun, J. Wang, Z. Qu, T. Wei, X. Liu, H. Sun, P.P. Monka, A. Hamza, Application of array Bessel beam generated by superposition method in electronic glass cutting, Opt Lasers Eng 181 (2024) 108384. https://doi.org/10.1016/J.OPTLASENG.2024.108384.
[11] C. Lutz, S. Schwarz, J. Marx, C. Esen, R. Hellmann, Multi-Bessel Beams Generated by an Axicon and a Spatial Light Modulator for Drilling Applications, Photonics 10 (2023) 413. https://doi.org/10.3390/PHOTONICS10040413.
[12] H. Cheng, C. Xia, S.M. Kuebler, P. Golvari, M. Sun, M. Zhang, X. Yu, Generation of Bessel-beam arrays for parallel fabrication in two-photon polymerization, J Laser Appl 33 (2021) 012040. https://doi.org/10.2351/7.0000313.
[13] J. Durnin, J. Miceli, J.H. Eberly, Diffraction-free beams, Phys Rev Lett 58 (1987) 1499. https://doi.org/10.1103/PhysRevLett.58.1499.
[14] G.A. Siviloglou, J. Broky, A. Dogariu, D.N. Christodoulides, Observation of accelerating airy beams, Phys Rev Lett 99 (2007) 213901. https://doi.org/10.1103/PhysRevLett.99.213901.
[15] R. Bowman, N. Muller, X. Zambrana-Puyalto, O. Jedrkiewicz, P. Di Trapani, M.J. Padgett, Efficient generation of Bessel beam arrays by means of an SLM, Eur Phys J Spec Top 199 (2011) 159–166. https://doi.org/10.1140/EPJST/E2011-01511-3.
[16] E. Stankevicius, M. Garliauskas, G. Raciukaitis, Bessel-like Beam Array Generation Using Round-tip Micro-structures and Their Use in the Material Treatment, Journal of Laser Micro Nanoengineering 11 (2016) 352–356. https://doi.org/10.2961/JLMN.2016.03.0013.
[17] X.Z. Wang, Q. Li, Z.P. Xiong, Z. Zhang, Q. Wang, Generation and scanning of Airy beams array by combining multiphase patterns, Appl Opt 52 (2013) 3039–3047. https://doi.org/10.1364/AO.52.003039.
[18] Z. Bouchal, J. Wagner, M. Chlup, Self-reconstruction of a distorted nondiffracting beam, Opt Commun 151 (1998) 207–211. https://doi.org/10.1016/S0030-4018(98)00085-6.
[19] S. Orlov, A. Juršėnas, J. Baltrukonis, V. Jukna, Controllable Spatial Array of Bessel-like Beams with Independent Axial Intensity Distributions for Laser Microprocessing, Journal of Laser Micro Nanoengineering 13 (2023) 324–329. https://doi.org/10.2961/jlmn.2018.03.0030.
[20] P. Šlevas, S. Orlov, Creating an Array of Parallel Vortical Optical Needles, Photonics 11 (2024). https://doi.org/10.3390/photonics11030203.
[21] P. Gotovski, P. Šlevas, S. Orlov, O. Ulčinas, A. Urbas, Generation of an optical needle beam with a laser inscribed Pancharatnam-Berry phase element under imperfect conditions, Opt Express 29 (2021) 33331. https://doi.org/10.1364/oe.438709.
[22] M.K. Bhuyan, K. Sugioka, Ultrafast Laser Micro and Nano Processing of Transparent Materials—From Fundamentals to Applications, in: P.M. Ossi (Ed.), Advances in the Application of Lasers in Materials Science, Springer International Publishing, Cham, 2018: pp. 149–190. https://doi.org/10.1007/978-3-319-96845-2_6.
[23] V. Garcés-Chávez, D. McGloin, H. Melville, W. Sibbett, K. Dholakia, Simultaneous micromanipulation in multiple planes using a self-reconstructing light beam, Nature 419 (2002) 145–147. https://doi.org/10.1038/nature01007.
[24] P. Polesana, M. Franco, A. Couairon, D. Faccio, P. Di Trapani, Filamentation in Kerr media from pulsed Bessel beams, Phys Rev A 77 (2008). https://doi.org/10.1103/PhysRevA.77.043814.
[25] R. Arimoto, C. Saloma, T. Tanaka, S. Kawata, Imaging properties of axicon in a scanning optical system, Appl Opt 31 (1992) 6653–6657. https://doi.org/10.1364/AO.31.006653.
[26] H. Cheng, C. Xia, M. Zhang, S.M. Kuebler, X. Yu, Fabrication of high-aspect-ratio structures using Bessel-beam-activated photopolymerization, Appl Opt 58 (2019) D91–D91. https://doi.org/10.1364/ao.58.000d91.
[27] M.K. Bhuyan, P.K. Velpula, J.P. Colombier, T. Olivier, N. Faure, R. Stoian, Single-shot high aspect ratio bulk nanostructuring of fused silica using chirp-controlled ultrafast laser Bessel beams, Appl Phys Lett 104 (2014). https://doi.org/10.1063/1.4861899/132247.
[28] F. He, J. Yu, Y. Tan, W. Chu, C. Zhou, Y. Cheng, K. Sugioka, Tailoring femtosecond 1.5-μm Bessel beams for manufacturing high-aspect-ratio through-silicon vias, Sci Rep 7 (2017). https://doi.org/10.1038/srep40785.
[29] J.H. McLeod, The axicon: a new type of optical element, J. Opt. Soc. Am. 44 (1954) 592–597. https://doi.org/10.1364/josa.44.000592.
[30] S. Schwarz, G.-L. Roth, S. Rung, C. Esen, R. Hellmann, Fabrication and evaluation of negative axicons for ultrashort pulsed laser applications, Opt Express 28 (2020) 26207. https://doi.org/10.1364/oe.401084.
[31] I. Golub, B. Chebbi, D. Shaw, D. Nowacki, Characterization of a refractive logarithmic axicon, Opt Lett 35 (2010) 2828.
[32] P. Boucher, J. Del Hoyo, C. Billet, O. Pinel, G. Labroille, F. Courvoisier, Generation of high conical angle Bessel–Gauss beams with reflective axicons, Appl Opt 57 (2018) 6725. https://doi.org/10.1364/ao.57.006725.
[33] S. Fujiwara, Optical Properties of Conic Surfaces. I. Reflecting Cone, J Opt Soc Am 52 (1962) 287.
[34] T. Tanaka, S. Yamamoto, Comparison of aberration between axicon and lens, n.d. www.elsevier.com/locate/optcom.
[35] Z. Bin, L. Zhu, Diffraction property of an axicon in oblique illumination, Appl Opt 37 (1998) 2563–2568. https://doi.org/10.1364/AO.37.002563.
[36] Z. Jaroszewicz, V. Climent, V. Duran, J. Lancis, A. Kolodziejczyk, A. Burvall, A.T. Friberg, Programmable axicon for variable inclination of the focal segment, J Mod Opt 51 (2004) 2185–2190. https://doi.org/10.1080/09500340408232522.
[37] S.N. Khonina, V. V. Kotlyar, V.A. Soifer, K. Jefimovs, P. Pääkkönen, J. Turunen, Astigmatic bessel laser beams, J Mod Opt 51 (2004) 677–686. https://doi.org/10.1080/09500340408235545.
[38] H. Cheng, C. Xia, S.M. Kuebler, X. Yu, Aberration correction for SLM-generated Bessel beams propagating through tilted interfaces, Opt Commun 475 (2020) 126213. https://doi.org/10.1016/J.OPTCOM.2020.126213.
[39] A. Thaning, Z. Jaroszewicz, A.T. Friberg, Diffractive axicons in oblique illumination: analysis and experiments and comparison with elliptical axicons, Appl Opt 42 (2003) 9–17. https://doi.org/10.1364/AO.42.000009.
[40] C. Ungaro, N. Kaliteevskiy, P. Sterlingov, V. V. Ivanov, A. Boh Ruffin, R.J. Terbrueggen, N. Savidis, Using phase-corrected Bessel beams to cut glass substrates with a chamfered edge, Appl Opt 60 (2021) 714. https://doi.org/10.1364/ao.413306.
[41] M. Jenne, D. Flamm, T. Ouaj, J. Hellstern, J. Kleiner, D. Grossmann, M. Koschig, M. Kaiser, M. Kumkar, S. Nolte, High-quality tailored-edge cleaving using aberration-corrected Bessel-like beams, Opt Lett 43 (2018) 3164–3167. https://doi.org/10.1364/OL.43.003164.
[42] P. Praharaj, M.K. Bhuyan, Nanosecond Laser Fabrication of Dammann Grating-like Structure on Glass for Bessel-Beam Array Generation, Photonics 11 (2024). https://doi.org/10.3390/photonics11050473.

Abbreviations: CW = Continuous Wave, SLM= Spatial Light Modulator, FWHM= Full Width at Half Maximum

[43] C. Wu, X. Huang, J. Yipeng, J. Wang, C.J. Chang-Hasnain, Subwavelength Bessel beam arrays with high uniformity based on a metasurface, Appl Opt 63 (2024) 2234. https://doi.org/10.1364/ao.519840.
[44] L. Chen, S. Kanwal, B. Yu, J. Feng, C. Tao, J. Wen, D. Zhang, Generation of high-uniformity and high-resolution Bessel beam arrays through all-dielectric metasurfaces, Nanophotonics 11 (2022) 967–977. https://doi.org/10.1515/nanoph-2021-0603.
[45] P. García-Martínez, M.M. Sánchez-López, J.A. Davis, D.M. Cottrell, D. Sand, I. Moreno, Generation of Bessel beam arrays through Dammann gratings, Appl Opt 51 (2012) 1375–1381.
[46] H. Pang, A. Cao, W. Liu, L. Shi, Q. Deng, Alternative Design of Dammann Grating for Beam Splitting With Adjustable Zero-Order Light Intensity, IEEE Photonics J 11 (2019) 1–9. https://doi.org/10.1109/JPHOT.2019.2899903.
[47] J. Dudutis, R. Stonys, G. Račiukaitis, P. Gečys, Aberration-controlled Bessel beam processing of glass, Opt Express 26 (2018) 3627. https://doi.org/10.1364/oe.26.003627.
[48] N. Ganguly, R. Dwivedi, C. D'Amico, R. Stoian, Asymmetric Shaping for Ultrafast Elliptical Bessel-like Beams, Photonics 10 (2023). https://doi.org/10.3390/photonics10060651.
[49] M. Jenne, D. Flamm, K. Chen, M. Schäfer, M. Kumkar, S. Nolte, Facilitated glass separation by asymmetric Bessel-like beams, Opt Express 28 (2020) 6552. https://doi.org/10.1364/oe.387545.

Abbreviations: CW = Continuous Wave, SLM= Spatial Light Modulator, FWHM= Full Width at Half Maximum